STED microscopy reveals that synaptotagmin remains clustered after synaptic vesicle exocytosis

Katrin I. Willig[1]*, Silvio O. Rizzoli[2]*, Volker Westphal[1], Reinhard Jahn[2] & Stefan W. Hell[1]

Synaptic transmission is mediated by neurotransmitters that are stored in synaptic vesicles and released by exocytosis upon activation. The vesicle membrane is then retrieved by endocytosis, and synaptic vesicles are regenerated and re-filled with neurotransmitter[1]. Although many aspects of vesicle recycling are understood, the fate of the vesicles after fusion is still unclear. Do their components diffuse on the plasma membrane, or do they remain together? This question has been difficult to answer because synaptic vesicles are too small (~40 nm in diameter) and too densely packed to be resolved by available fluorescence microscopes. Here we use stimulated emission depletion (STED)[2] to reduce the focal spot area by about an order of magnitude below the diffraction limit, thereby resolving individual vesicles in the synapse. We show that synaptotagmin I, a protein resident in the vesicle membrane, remains clustered in isolated patches on the presynaptic membrane regardless of whether the nerve terminals are mildly active or intensely stimulated. This suggests that at least some vesicle constituents remain together during recycling. Our study also demonstrates that questions involving cellular structures with dimensions of a few tens of nanometres can be resolved with conventional far-field optics and visible light.

Synaptic vesicle recycling has been studied for over three decades[3,4]. In the best documented model of neurotransmitter release, the synaptic vesicle membrane undergoes exocytosis by collapsing into the plasma membrane[4], referred to as full fusion. Fusion is thought to involve, at least to some extent, mixing and lateral diffusion of vesicle proteins across the plasma membrane before they are re-internalized by endocytosis. Accordingly, to regenerate vesicles, sorting of these proteins must occur at the plasma membrane and/or in an endosomal intermediate[1,5,6]. However, if vesicle constituents remain patched together after exocytosis, the recycling machinery would just have to internalize the fused vesicular patch without elaborate sorting. To date, it has not been possible to differentiate between these alternatives. Owing to their diffraction-limited resolution, confocal and epifluorescence microscopes cannot identify single-vesicle-derived protein patches in a synaptic bouton; moreover, individual vesicles are also impossible to image, except under sparse labelling conditions[7–9]. Electron microscopy, on the other hand, provides sufficient resolution, but the required labelling efficiency has hitherto not been achievable.

Recent advances in optical physics have shown that the diffraction barrier of far-field fluorescence microscopy can be broken by stimulated emission depletion (STED)[2,10,11]. In fact, STED is just one example of a family of microscopy concepts that, in spite of using regular lenses, allow diffraction-unlimited resolution[11–13]. In a typical STED microscope the excitation beam is overlapped with a doughnut-shaped beam that is capable of de-exciting fluorophores by stimulated emission. Co-alignment of the beams ensures that fluorescence is allowed only in the central area of the excitation spot where the doughnut beam is close to zero (Fig. 1a). Scanning with a narrowed spot across the sample readily yields subdiffraction images. With a sufficiently intense doughnut, the fluorescent spot of a STED microscope can, in principle, be sharpened down to the molecular scale[2,11,12].

To investigate synaptic vesicle recycling in cultured neurons, we built a STED microscope with an objective lens of 1.4 numerical aperture. The green-emitting dye used for antibody labelling was excited at 470 nm and de-excited at 615 nm. Without STED, the full-width-half-maximum (FWHM) of the fluorescent focal spot was 195 nm, which is typical for a first-rate confocal microscope[14]. Applying the doughnut of our setup yielded a spot FWHM of 66 nm (Fig. 1a), corresponding to a ninefold reduction in the effective focal area. Moreover, the spot of the STED microscope becomes increasingly thinner towards the top[12], implying that the resolution is slightly better. Simulations revealed that given the encountered noise conditions, our STED microscope allows the separation of point objects that are 45 nm apart in the focal plane, which is sufficient for resolving individual synaptic vesicles within nerve terminals.

For imaging, vesicles were targeted with a monoclonal antibody directed against the intravesicular domain of the synaptic vesicle protein synaptotagmin[15] (Fig. 1b). Figure 1c shows an epifluorescence overview image of primary cultured hippocampal neurons incubated with the antibody at 37 °C for 5 min. Upon neuronal activity, a vesicle opens to the outside space (exocytosis), rendering its inside accessible to the antibodies. These bind to the synaptotagmin molecules and are internalized when the vesicles are retrieved[16]. Thus, only vesicles undergoing exocytosis during the incubation time are labelled. These vesicles were visualized by fluorescently labelled secondary antibodies applied after membrane permeabilization and fixation. The gain in resolution becomes apparent by comparing the panels in Fig. 1d showing confocal and STED microscopy images. Whereas the former does not show substructures below the level of individual boutons, the latter resolves numerous dots within the terminals.

To differentiate between the synaptotagmin pool remaining on the surface of the plasma membrane and that internalized by endocytosis, we used two different protocols. First, labelling was performed on ice and in the absence of Ca^{2+}; that is, conditions under which no endocytosis occurs. Bright staining was observed (Fig. 2a). Second, labelling was performed at 37 °C to allow for uptake, resulting in antibody binding to both surface-exposed and internalized synaptotagmin pools. To selectively label the internalized pool, we blocked the surface-bound antibodies with unlabelled secondary antibodies before adding dye-labelled secondary antibodies. As we expected, the staining intensity of blocked, non-permeabilized preparations was hardly above background (Fig. 2b). Conversely, strong labelling was observed after permeabilization,

[1]Departments of NanoBiophotonics and [2]Neurobiology, Max Planck Institute for Biophysical Chemistry, 37077 Göttingen, Germany.
*These authors contributed equally to this work.

showing that the internalized (unblocked) vesicles were accessible to secondary antibody labelling (Fig. 2c). To further ensure that internal epitopes were only accessible after permeabilization, we labelled neurons with an antibody specific for the cytoplasmic tail of synaptotagmin[17]. Labelling was only observed when cultures were permeabilized before antibody incubation (Fig. 2e, f).

A comparison of surface-exposed and internalized synaptotagmin pools as resolved by STED microscopy is shown in Fig. 2g, h. Both the internalized and the surface-exposed pools were resolved as confined dots. Thus, synaptotagmin remains concentrated in small clusters after exocytosis instead of being dispersed across the plasma membrane. Furthermore, there were consistently fewer dots detectable on the surface compared with the internalized pool, indicating that the plasma membrane pool is short-lived owing to rapid endocytosis. Notably, the dots on the cell surface appeared brighter than those of the internalized pool. We therefore quantified dot brightness (see Methods). For comparison, a dilute solution of primary antibodies was adsorbed on glass, labelled with secondary antibodies, imaged by STED, and quantified in parallel. The resulting histogram (Fig. 2i) shows (1) that both internalized and surface-exposed dots are significantly brighter than individual antibodies, confirming that each dot represents multiple synaptotagmin molecules, and (2) that the brightness of the surface-exposed patches is shifted towards higher values compared to the internalized vesicles. The second observation is probably due to the brevity of the endocytic process (2–5 s; ref. 18), which limits epitope accessibility for the antibodies. Surface patches, on the other hand, were exposed to the antibody solution for a few minutes (on ice, to inhibit active recycling), resulting in a higher labelling efficiency. Comparison of the internalized pool with the total (unblocked) pool after permeabilization

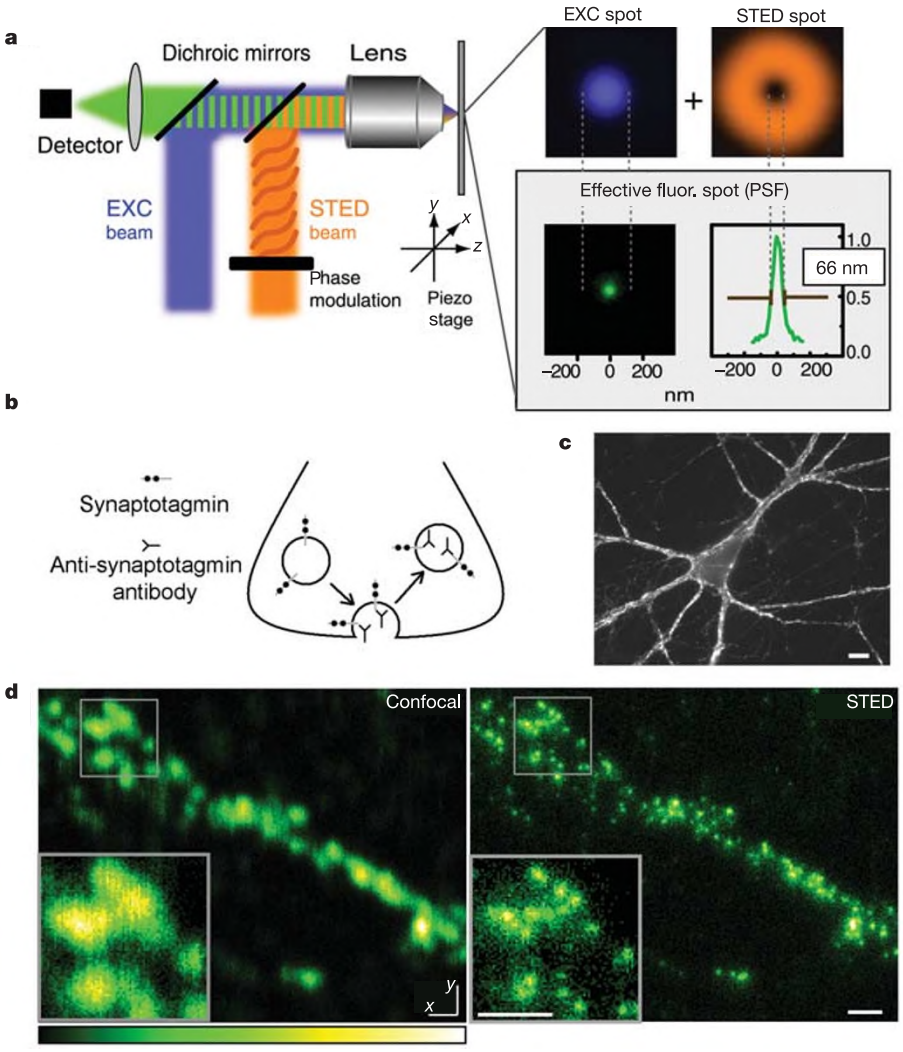

Figure 1 | STED microscopy resolves synaptic vesicles in individual boutons of primary cultured hippocampal neurons. **a**, Principles of operation. While the blue excitation (EXC) beam is focused to a diffraction-limited excitation spot, shown in the adjacent panel in blue, the orange STED beam is able to de-excite molecules. The STED beam is phase-modulated to form the focal doughnut shown in the top right panel. Superimposition of the two focal spots confines the area in which fluorescence is possible to the doughnut centre, yielding the effective fluorescent spot of subdiffraction size shown in green in the lower panel. All spots represent measured data and are drawn to scale. The profile of the green effective fluorescent spot has an FWHM of 66 nm as well as a sharp peak. The green spot shows an 11-fold reduction in focal area beyond the excitation diffraction value (compare with blue spot). **b**, Mechanism of synaptic labelling. Synaptic vesicles exocytose, allowing their lumenal synaptotagmin domains to bind anti-synaptotagmin antibodies. These antibodies are internalized upon endocytosis. **c**, Typical image of a neuron labelled with an anti-synaptotagmin antibody, fixed, permeabilized and visualized using Atto 532-labelled secondary antibodies. Fluorescent puncta represent labelled synaptic nerve terminals. Scale bar, 10 μm. **d**, Comparison of confocal (left) and STED (right) counterpart images of a labelled preparation reveals a marked increase in resolution by STED. Scale bar, 500 nm.

revealed that a significant fraction of brighter (surface?) dots is preserved, suggesting that permeabilization does not disrupt the surface clusters (Supplementary Fig. S1).

We next strongly stimulated our preparations (using 70 mM KCl) in the presence of anti-synaptotagmin antibodies. Permeabilization of the preparations revealed intense staining, suggesting that many vesicles had been labelled. Total surface fluorescence also increased more than twofold (not shown). However, the staining pattern of the surface pools was very similar to the unstimulated cultures (Fig. 3a, b), indicating that synaptotagmin remains clustered even during high synaptic activity.

We then asked whether the surface dots represent the synaptotagmin inventory of individual vesicles, or whether they represent (at least in part) aggregated patches. As brightness alone cannot be used as a criterion, we compared the dot diameters of the internalized pool with those of the surface pool (Fig. 3c and Supplementary Fig. S2). All populations peaked at 70–85 nm, with no significant differences among them. Considering the 35–40 nm vesicle diameter observed with electron microscopy[19] and the spot size of our STED microscope, we anticipated a dot diameter of ~70 nm. The minority of slightly larger diameters might be due to the bound antibody sandwich. Thus, the observed values are in agreement with values predicted for a membrane patch derived from a single vesicle (Supplementary Fig. S3).

Although our data strongly suggest that synaptotagmin remains clustered after exoytosis, we cannot rule out that the proteins disperse briefly before being re-clustered. However, we regard this option as unlikely because there are only a few spots on the surface that correspond in intensity to single molecules. Previous observations have suggested the dispersal of a vesicle protein (green fluorescent protein (GFP)-tagged synaptobrevin) out of nerve terminals into the axons upon strong stimulation[20]. However, it remained uncertain whether the dispersal was due to diffusion of patches or of single molecules. If we further incubate surface-labelled preparations to allow for endocytosis before adding the membrane-impermeant detection reagent, staining is strongly reduced (see Supplementary Fig. S4). Thus, the patches are ultimately endocytosed, possibly through interaction with synaptotagmin[21].

At present, we do not know whether the behaviour of synaptotagmin is a paradigm for all vesicle proteins. However, vesicle proteins have been reported to adhere to one another after solubilization in various detergents[22]. Thus, it is conceivable that other vesicle constituents remain associated with synaptotagmin in the plasma membrane when recycling, both at rest and during high neuronal activity. Our findings may also explain the quantal character of vesicle endocytosis described in ref. 7—if the synaptic vesicle components remain clustered in the membrane, it is easy to envisage how endocytosis (and not only exocytosis) can assume quantal behaviour.

Our application of subdiffraction far-field optical resolution to an unsolved problem in cell biology holds great promise for addressing other questions involving dimensions on the scale of tens of nanometres. Maintaining both the labelling efficiency of fluorescence microscopy and its ease of operation, STED should provide an alternative to electron microscopy. Importantly, STED is a purely physical phenomenon; no mathematical data processing is required for the image generation. We also note that the 45–66 nm resolution reported here does not represent a limit in biological imaging. Being inherently diffraction-unlimited, the resolution of a STED microscope can be further increased by optimizing STED and/or the doughnut. In fact, a focal spot width of 16 nm has recently been measured in single-molecule experiments[23]. Therefore, our study not only provides insights into the mechanisms of vesicle recycling, but also demonstrates the power of an emerging family of microscopy techniques that, despite using regular objective lenses and visible light, is no longer limited by diffraction.

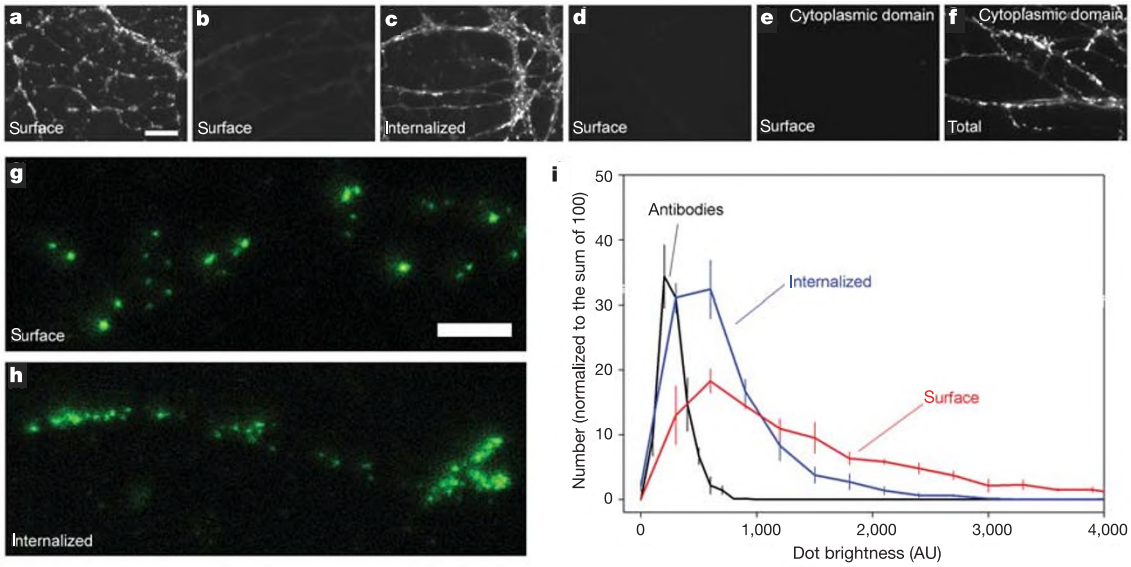

Figure 2 | Comparison between surface-exposed and internalized pools of synaptotagmin shows that the protein remains clustered in the presynaptic plasma membrane. **a**–**f**, Widefield images of hippocampal neurons labelled with antibodies specific for the lumenal (**a**–**d**) or cytoplasmic (**e**, **f**) domain of synaptotagmin. **a**, Selective staining of the surface pool (low temperature and no calcium, to prevent endocytosis during labelling). **b**, Surface staining as in **a** but with secondary antibody added after blocking the surface epitopes of the bound monoclonal antibody using unlabelled anti-mouse antibodies (negative control). **c**, Selective staining of the internalized pool (labelled under conditions of active endocytosis followed by surface blocking as in **b**, but permeabilized after fixation). **d**, Cultures stained with secondary antibodies only. **e**, **f**, Controls showing that an antibody specific for the cytoplasmic domain of synaptotagmin has no access to the epitope (**e**) unless the preparation is permeabilized after fixation (**f**). Scale bar, 10 μm. **g**, STED image of surface-stained synapses (conditions as in **a**). Scale bar, 1 μm. **h**, STED image of internalized vesicles (conditions as in **c**). **i**, Quantification of the brightness of single dots (in arbitrary units), compared with the dot brightness derived from single primary antibodies adsorbed to glass (see Methods). The graphs represent averages of 3–5 independent experiments (±s.e.m.). Note that the bin size is 100 units for the single antibody graph and 300 units for the other images.

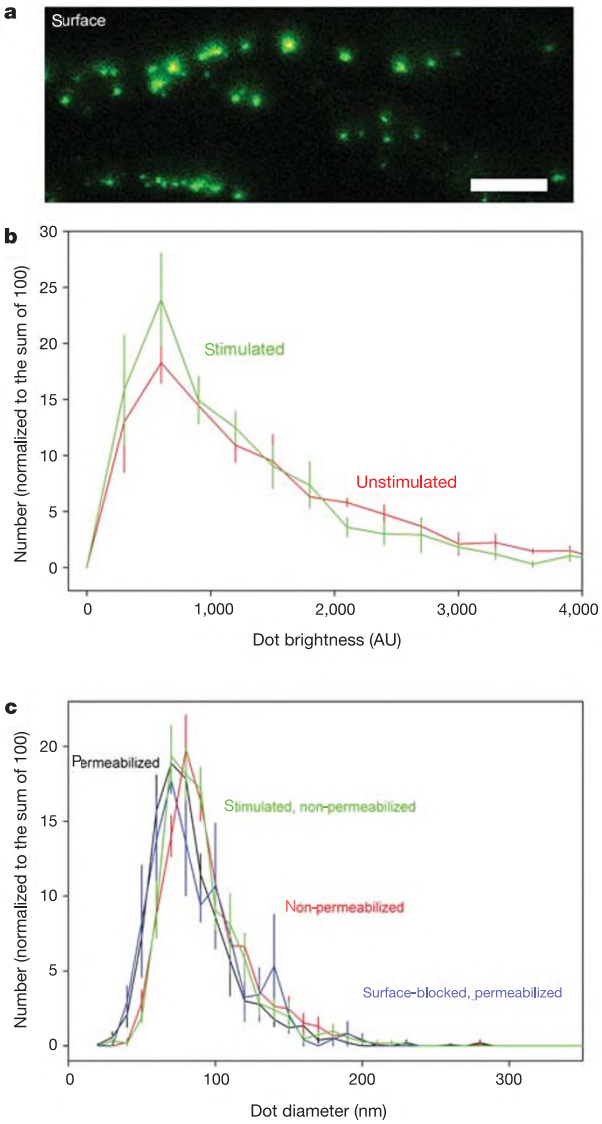

Figure 3 | Dot sizes of surface-exposed and internalized synaptotagmin pools do not show major differences, and neither dot brightness nor dot sizes change upon stimulation of exocytosis. a, Typical STED image of a heavily stimulated, surface-stained, non-permeabilized preparation. Compare with Fig. 2g. Scale bar, 1 μm. **b**, Comparison of dot brightness of the surface pool in stimulated and unstimulated preparations (mean ± s.e.m. from 4–5 independent experiments). **c**, Quantification of dot FWHM for different preparations (see Methods). We analysed the dots from 3–5 different experiments. To ensure that dot FWHM measurements were not affected by dots that were closely together, a stringent χ^2 cutoff of less than 0.01 (difference between the fit and the data) was placed on the lorentzian fit to the dots. See also Supplementary Fig. S2.

METHODS

Primary cultures. Primary cultures of hippocampal neurons were prepared from newborn rats (following procedures in refs 24, 25) and were used between days 15 and 25 *in vitro*. We used cultures plated onto astrocytic monolayers as well as cultures plated directly onto coverslips, with identical results. For antibody labelling, the neurons were incubated with a solution of anti-synaptotagmin monoclonal antibody (604.1, ref. 15) for 5 min at either 37 °C or on ice (for selective surface staining) in a Tyrode solution containing 124 mM NaCl, 5 mM KCl, 2 mM $CaCl_2$, 1 mM $MgCl_2$, 30 mM glucose and 25 mM HEPES (pH 7.4), washed briefly and fixed with 4% paraformaldehyde in PBS containing 1 mM EGTA. Where indicated, we stimulated the cultures at 37 °C in the presence of anti-synaptotagmin antibodies, in normal buffer containing calcium, before fixation. Surface-selective staining was then achieved by applying the secondary antibodies in the absence of permeabilization. After washing, sheep anti-mouse Atto 532-labelled antibodies were added for 2 h at 22 °C; the cultures were then mounted in Mowiol (containing 6 g glycerol AR (4094, Merck), 2.4 g Mowiol 4-88 (Hoechst), 6 ml H_2O, 12 ml 0.2 M Tris pH 7.2 buffer) and imaged. Permeabilization was achieved using 0.1% Triton X-100 after fixation. The use of monoclonal (rather than polyclonal) antibodies ensures that any molecular patches observed cannot result from antibody-induced clustering. For investigation of the signal coming from single primary antibodies, coverslips treated with poly-L-lysine were incubated with anti-synaptotagmin antibodies for 30 min, fixed, washed, incubated with secondary antibodies and mounted. For the experiments in Fig. 2e, f, we used monoclonal antibody 41.1, which is directed against the cytoplasmic domain of synaptotagmin[17].

Conventional imaging. Wide-field images were obtained with an epifluorescence microscope. The rhodamine dye Atto 532 was detected using a 480/20 excitation filter, a 530 DCLP beamsplitter and a 560/40 emission filter. For detection of Cy3 fluorescence (Fig. 2e, f) a 565/30 excitation filter, 595 DCLP beamsplitter and 645/745 emission filter were used (all filters were obtained from AHF Analysentechnik). Cy 3-labelled goat anti-mouse secondary antibodies were obtained from Jackson Immunoresearch.

STED microscopy. STED microscopy was performed with a home-built setup. Dye excitation was accomplished with a laser diode (Picoquant) emitting 100-ps pulses. The diode was triggered by STED pulses delivered by an optical parametric oscillator (APE) that was sychronously pumped by a Ti:Sapphire laser (MaiTai, Spectra Physics) operating at 80 MHz. The STED pulses were stretched to 200 ps by dispersion in a glass fibre and converted into a focal doughnut by means of a spatial light modulator (Hamamatsu) delivering a helical phase ramp (0–2π) with a central singularity[26]. Both beams were coupled into an oil immersion lens (HCX PL APO, ×100, Leica) using custom-designed dichroic mirrors. The average power of the excitation and STED beams at the sample was 2 μW and 14 mW, respectively. The fluorescence collected by the lens was imaged onto a counting avalanche photodiode with an opening diameter of 71% of that of the back-projected fluorescence spot. STED-imaging was obtained by piezo-scanning the sample at a pixel dwell time of ~0.3 ms. With a pixel size of $15 \times 15\,nm^2$, the recording of a $1 \times 1\,\mu m^2$ area involved an effective exposure time of 1.4 s.

The spot size and hence the resolution Δr of a STED microscope follows a new law $\Delta r \cong \lambda / \left(2n \sin\alpha \sqrt{1 + I/I_{sat}}\right)$, where λ and $n \sin\alpha$ denote the wavelength and numerical aperture of the lens, respectively[11,13,23]. I is the maximal focal intensity applied for STED and I_{sat} is a characteristic value at which the fluorescence probability is reduced to ~1/e. Unlike in a confocal or epifluorescence light microscope, for $I/I_{sat} \to \infty$ it follows that $\Delta r \to 0$, meaning that the resolution is no longer limited by diffraction.

Fluorescence labelling. For the secondary antibody, the green-emitting dye Atto 532 (a gift from K. H. Drexhage) was coupled to an anti-mouse IgG (Jackson ImmunoResearch) via its succinimidyl ester.

Data analysis. Dot brightness and FWHM were evaluated with macros in MatLab (Mathworks). The user interactively defined a region enclosing the dot of fluorescence in the image. The background level and the FWHM of focal spots in the *x*- and *y*-direction were derived from lorentzian fits. The brightness was defined as the background-corrected sum over all pixels within the FWHM. Averages of the values for the dots in the *x*- and *y*-directions were retained for each dot. Graphs show histograms of FWHM and brightness as mean ± s.e.m.

1. Sudhof, T. C. The synaptic vesicle cycle. *Annu. Rev. Neurosci.* **27,** 509–547 (2004).
2. Hell, S. W. & Wichmann, J. Breaking the diffraction resolution limit by stimulated emission: stimulated emission depletion microscopy. *Opt. Lett.* **19,** 780–782 (1994).
3. Ceccarelli, B., Hurlbut, W. P. & Mauro, A. Turnover of transmitter and synaptic vesicles at frog neuromuscular junction. *J. Cell Biol.* **57,** 499–524 (1973).
4. Heuser, J. E. & Reese, T. S. Evidence for recycling of synaptic vesicle membrane during transmitter release at frog neuromuscular junction. *J. Cell Biol.* **57,** 315–344 (1973).
5. Rizzoli, S. O. & Betz, W. J. Synaptic vesicle pools. *Nature Rev. Neurosci.* **6,** 57–69 (2005).
6. Royle, S. J. & Lagnado, L. Endocytosis at the synaptic terminal. *J. Physiol. (Lond.)* **553,** 345–355 (2003).
7. Gandhi, S. P. & Stevens, C. F. Three modes of synaptic vesicular recycling revealed by single-vesicle imaging. *Nature* **423,** 607–613 (2003).
8. Aravanis, A. M., Pyle, J. L. & Tsien, R. W. Single synaptic vesicles fusing transiently and successively without loss of identity. *Nature* **423,** 643–647 (2003).
9. Zenisek, D., Steyer, J. A., Feldman, M. E. & Almers, W. A membrane marker

leaves synaptic vesicles in milliseconds after exocytosis in retinal bipolar cells. *Neuron* **35,** 1085–1097 (2002).
10. Klar, T. A., Jakobs, S., Dyba, M., Egner, A. & Hell, S. W. Fluorescence microscopy with diffraction resolution limit broken by stimulated emission. *Proc. Natl Acad. Sci. USA* **97,** 8206–8210 (2000).
11. Hell, S. W. Toward fluorescence nanoscopy. *Nature Biotechnol.* **21,** 1347–1355 (2003).
12. Hell, S. W. in *Topics in Fluorescence Spectroscopy* (ed. Lakowicz, J. R.) 361–422 (Plenum Press, New York, 1997).
13. Hell, S. W. Strategy for far-field optical imaging and writing without diffraction limit. *Phys. Lett. A* **326,** 140–145 (2004).
14. Wilson, T. & Sheppard, C. J. R. *Theory and Practice of Scanning Optical Microscopy* (Academic, New York, 1984).
15. Chapman, E. R. & Jahn, R. Calcium-dependent interaction of the cytoplasmic region of synaptotagmin with membranes. Autonomous function of a single C2-homologous domain. *J. Biol. Chem.* **269,** 5735–5741 (1994).
16. Kraszewski, K. *et al.* Synaptic vesicle dynamics in living cultured hippocampal-neurons visualized with Cy3-conjugated antibodies directed against the lumenal domain of synaptotagmin. *J. Neurosci.* **15,** 4328–4342 (1995).
17. Brose, N., Petrenko, A. G., Sudhof, T. C. & Jahn, R. Synaptotagmin: a calcium sensor on the synaptic vesicle surface. *Science* **256,** 1021–1025 (1992).
18. Pyle, J. L., Kavalali, E. T., Piedras-Renteria, E. S. & Tsien, R. W. Rapid reuse of readily releasable pool vesicles at hippocampal synapses. *Neuron* **28,** 221–231 (2000).
19. Harris, K. M. & Sultan, P. Variation in the number, location and size of synaptic vesicles provides an anatomical basis for the nonuniform probability of release at hippocampal CA1 synapses. *Neuropharmacology* **34,** 1387–1395 (1995).
20. Sankaranarayanan, S. & Ryan, T. A. Real-time measurements of vesicle-SNARE recycling in synapses of the central nervous system. *Nature Cell Biol.* **2,** 197–204 (2000).
21. Poskanzer, K. E., Marek, K. W., Sweeney, S. T. & Davis, G. W. Synaptotagmin I is necessary for compensatory synaptic vesicle endocytosis *in vivo*. *Nature* **426,** 559–563 (2003).
22. Bennett, M., Calakos, N., Kreiner, T. & Scheller, R. Synaptic vesicle membrane proteins interact to form a multimeric complex. *J. Cell Biol.* **116,** 761–775 (1992).
23. Westphal, V. & Hell, S. W. Nanoscale resolution in the focal plane of an optical microscope. *Phys. Rev. Lett.* **94,** 143903 (2005).
24. Rosenmund, C. & Stevens, C. F. The rate of aldehyde fixation of the exocytotic machinery in cultured hippocampal synapses. *J. Neurosci. Methods* **76,** 1–5 (1997).
25. Klingauf, J., Kavalali, E. T. & Tsien, R. W. Kinetics and regulation of fast endocytosis at hippocampal synapses. *Nature* **394,** 581–585 (1998).
26. Török, P. & Munro, P. R. T. The use of Gauss-Laguerre vector beams in STED microscopy. *Opt. Expr.* **12,** 3605–3617 (2004).

Supplementary Information is linked to the online version of the paper at www.nature.com/nature.

Acknowledgements The authors thank E. Neher for helpful comments. S.O.R. acknowledges fellowships from the European Molecular Biology Organization and from the Human Frontier Science Program. This work was partly supported by a grant from the Leibniz Program of the Deutsche Forschungsgemeinschaft awarded to R.J., a grant from the German Ministry of Research and Education to S.W.H., and by the DFG-Centre for Molecular Physiology of the Brain. We thank I. Herefort, M. Wienisch and J. Klingauf for assistance with cell culturing, and A. Schönle for help with his software ImSpector.

Author Information Reprints and permissions information is available at npg.nature.com/reprintsandpermissions. The authors declare no competing financial interests. Correspondence and requests for materials should be addressed to R.J. (rjahn@gwdg.de).